Int. J. Heat Mass Transfer. Vol. 35, No. 3, pp. 605–612, 1992
Printed in Great Britain

0017–9310/92 $5.00 + 0.00
Pergamon Press plc

The photoacoustic technique as a convenient instrument to determine thermal diffusivities of gases†

K. STEPHAN and J. BIERMANN

Institut für Technische Thermodynamik und Thermische Verfahrenstechnik,
Universität Stuttgart, Pfaffenwaldring 9, 7000 Stuttgart 80, F.R.G.

Abstract—The thermal diffusivity of gases can be determined with a method based upon the photoacoustic effect. The theoretical fundamentals of the photoacoustic technique for thermal diffusivity measurements are presented and a photoacoustic cell designed for accurate measurements over the temperature range from 290 up to 423 K at atmospheric pressure is described. The average absolute deviation of the experimental data from recommended data, for gaseous argon, does not exceed 1%.

1. INTRODUCTION

THERMAL diffusivities of fluids can be determined by direct measurements, e.g. by the transient hot-wire technique [1, 2] and the dynamic light scattering method [3–6], or indirectly by calculation from individual experimental data of thermal conductivity, density, and isochoric or isobaric heat capacity. The indirect method is only applicable if reliable individual data of thermal conductivity, density, and heat capacity are accessible. However, thermal conductivities near the critical point and in the range of low densities, as well as heat capacities in the critical region, are difficult to measure. Alternatively, thermal diffusivities can be obtained more easily by direct measurements which often yield better accuracies than the indirect method. At present, the accuracy that can be attained in thermal diffusivity measurements with the transient hot-wire technique is of the order of 7–9% [7], whereas recently presented thermal diffusivities of R22 and R134a determined by the dynamic light scattering method [8] show an overall error of approximately 2.0%. Both experimental techniques cannot be applied in the region of low densities.

In a recent paper Stephan *et al.* [9] presented a new technique based upon the photoacoustic effect as a convenient method to determine thermal diffusivities of fluids at low densities. They presented experimental results for different gases at 0.1 MPa and 293 K. The main advantage of the photoacoustic technique is the very small temperature gradient of a few mK. Thus errors caused by convection and radiation are avoided.

The experimental set-up described in ref. [9] served only as a test device to demonstrate that thermal diffusivities of gases can be measured with sufficient accuracy by the photoacoustic technique. Experiments conducted with that apparatus were limited to ambient temperature and pressure. In the present paper, an improved photoacoustic cell for measurements up to 423 K at ambient pressure (0.1 MPa) is described. In addition, an extended analysis is given which results in an equation for the evaluation of the thermal diffusivity from the photoacoustic signal. At present, measurements cannot be extended to higher pressures because high-sensitive microphones for the detection of the photoacoustic signal operating at pressures above 0.1 MPa are not available.

In order to demonstrate the applicability of the photoacoustic technique for thermal diffusivity measurements at higher temperatures, experiments with argon were carried out in the temperature range from 295 up to 423 K.

2. PHOTOACOUSTIC EFFECT

The photoacoustic effect by definition is based upon the conversion of radiation energy into an acoustic signal. In the experiments we used a continuous wave He–Ne laser as coherent radiation source equipped with special mirrors which delivered an emission wavelength of 3.4 μm. At this wavelength all alkanes, particularly ethane, show a strong absorption line. Small amounts of ethane (between 500 and 1000 ppm) added to the pure gas provide sufficient absorption without affecting the thermophysical properties of the pure substance. Thus, with ethane as an absorbing substance, the measurements can be performed independently of fluid-specific absorption lines.

The absorption of radiation causes the ethane molecules to pass into excited vibrational states. The excited molecules then relax to their ground state within a few microseconds, transforming vibrational energy into translational energy by inelastic collisions with surrounding molecules. The energy transfer provokes a small rise of temperature and pressure in the sample.

† Dedicated to Professor Dr.-Ing. Dr.-Ing.e.h. Ulrich Grigull.

NOMENCLATURE

A	heat production [W m^{-3}]
a	thermal diffusivity [m^2 s^{-1}]
B	parameter, equation (9)
b	laser beam radius [m]
C	parameter, equation (3)
C_m	coefficients, $m = 1, 2, \ldots, \infty$, equation (6)
c_v	isochoric specific heat capacity [J kg^{-1} K^{-1}]
D_m	parameter, $m = 1, 2, \ldots, \infty$, equation (10)
I	intensity of laser beam [W m^{-2}]
J_0	Bessel function, zero order
J_1	Bessel function, first order
K_m	coefficients, $m = 1, 2, \ldots, \infty$, equation (12)
L	length of gas sample chamber [m]
M	molar mass [kg mol^{-1}]
p	pressure [Pa]
R	radius of cylindrical sample chamber [m]
$\mathbb{R}$	universal gas constant [J mol^{-1} K^{-1}]
r	radius [m]
T	temperature [K]
t	time [s]
W	radiation power of the laser [W]
w	beam radius [m]
w_0	minimum beam radius [m]
x	dimensionless radius, $x = r/R$
z	axial coordinate [m].

Greek symbols

α	absorptivity coefficient [m^{-1}]
Δp	pressure rise, $\Delta p(t) = p(t) - p_0$ [Pa]
ΔT	local temperature rise, $\Delta T(t, r, z) = T(t, r, z) - T_0$ [K]
$\Delta\bar{T}$	average temperature rise, $\Delta\bar{T}(t) = \bar{T}(t) - T_0$ [K]
κ	isentropic exponent
λ	thermal conductivity [W m^{-1} K^{-1}]
λ^*	radiation wavelength [m]
ξ_m	roots of the Bessel function, zero order, $J_0(\xi_m) = 0$
ρ	density [kg m^{-3}].

Subscripts

0	initial ($t = 0$)
∞	for infinite time ($t \to \infty$).

Periodical modulation of the radiation leads to pressure fluctuations which can be detected by a sensitive microphone (Fig. 1). The thermal diffusivity of the sample gas can be calculated from the time-dependent pressure rise.

3. ANALYSIS

The basic equation for the evaluation of the thermal diffusivity from a photoacoustic signal was given in an earlier paper [9]. In the present paper the analysis is extended insofar as the intensity distribution of the laser beam is taken into account. Thus an improved quantitative description of the pressure rise is derived, permitting a more accurate determination of the thermal diffusivity.

The pressure rise as a function of time can be calculated from the average time-dependent temperature rise. The temperature rise is obtained from the equation of heat conduction in an infinite cylinder, because the sample chamber of the photoacoustic cell is a narrow cylindrical tube with a length-to-diameter ratio of 65

$$\lambda\left(\frac{\partial^2 T}{\partial r^2} + \frac{1}{r}\frac{\partial T}{\partial r}\right) = \rho c_v \frac{\partial T}{\partial t} - A(r). \tag{1}$$

Herein λ denotes the thermal conductivity, ρ the density, c_v the isochoric heat capacity, and T the temperature of the sample gas. The heat generation term A is determined from the part of the laser beam intensity absorbed by the sample gas. In the basic analysis [9] the heat generation A was assumed constant. Instead, the intensity distribution of an ideal laser beam obeys a Gaussian function (Fig. 2) according to

$$I(r, z) = \frac{W}{\pi w(z)^2} \exp\left(-\frac{r^2}{w(z)^2}\right) \tag{2}$$

with W as the radiation power of the laser and its

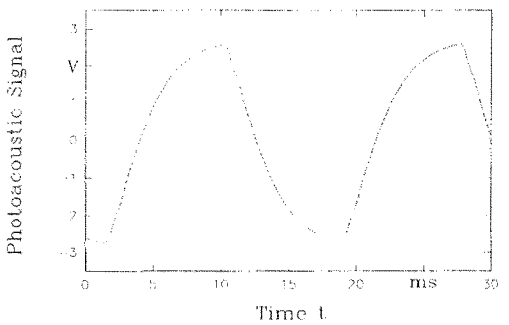

FIG. 1. Pressure signal vs time.

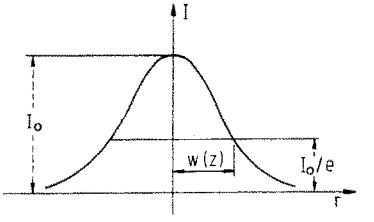

FIG. 2. Intensity profile of the laser beam.

beam radius $w(z)$ defined as the radius at which the intensity of the beam is $1/e$ of its peak value. Beam radii $w(z)$ were measured by a beam scanner along the propagation path of the beam. Beam radii follow a hyperbolic relationship [10] (Fig. 3), along the axis of the tube

$$w(z) = w_0[1+Cz^2]^{0.5} \tag{3}$$

with the minimum spot w_0 located in the center of the tube. Evaluation of our measurements yielded $w_0 = 182\ \mu\text{m}$ and $C = 5.0\times 10^2\ \text{m}^{-2}$. Thus the heat generation term A as a function of the radius r and the distance z along the beam path is given by

$$A(r,z) = \alpha I(r,z) = \frac{\alpha W}{\pi w(z)^2}\exp\left(-\frac{r^2}{w(z)^2}\right) \tag{4}$$

where α denotes the absorption coefficient. The solution of equation (1) with the heat generation function A, equation (4), initial temperature T_0, and $T(t, R, z) = T_0$ is [11]

$$T(t,r,z) = T_0+\Delta T(t,r,z) = T_0 + \left(\frac{\alpha W}{4\pi\lambda}\right)\left[\sum_{n=1}^{\infty}(-1)^n\left(\left(\frac{r}{R}\right)^{2n}-1\right)\left(n!n\left(\frac{w}{R}\right)^{2n}\right)^{-1} + \sum_{m=1}^{\infty} C_m J_0\left(\xi_m\frac{r}{R}\right)\exp\left(-\frac{\xi_m^2 at}{R^2}\right)\right]. \tag{5}$$

ξ_m are the roots of the Bessel function of zero order, $J_0(\xi_m) = 0$, and R is the radius of the cylindrical sample chamber. The boundary condition of a constant temperature T_0 at the cylinder wall is justified because of the high thermal conductivity and heat capacity of the wall material compared to the respective values of the sample gas. The coefficients C_m are given by

$$C_m = -\frac{2}{J_1^2(\xi_m)}\left[\sum_{n=1}^{\infty}(-1)^n\left(n!n\left(\frac{w}{R}\right)^{2n}\right)^{-1} \times\left(\int_0^1 (x^{2n+1}-x)J_0(\xi_m x)\,dx\right)\right] \tag{6}$$

with the dimensionless radius $x = r/R$ and the Bessel function of first order J_1. The thermal diffusivity a is defined as

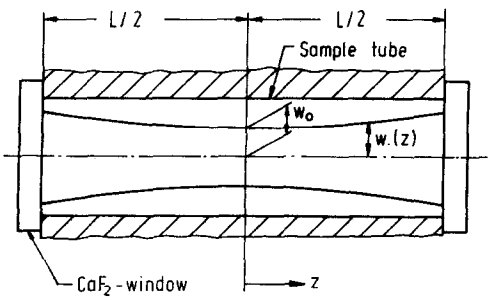

FIG. 3. Contour of the Gaussian beam.

$$a = \lambda/\rho c_v. \tag{7}$$

Integration of equation (5) yields the average time-dependent temperature rise $\Delta\bar{T}(t) = \bar{T}(t)-T_0$ of the sample gas

$$\Delta\bar{T}(t) = \frac{4}{R^2L}\int_0^{L/2}\int_0^R \Delta T(t,r,z)r\,dr\,dz = \left(\frac{\alpha W}{4\pi\lambda}\right)\left[B+\sum_{m=1}^{\infty} D_m\exp\left(-\frac{\xi_m^2 at}{R^2}\right)\right] \tag{8}$$

with

$$B = \frac{4}{R^2L}\int_0^R\int_0^{L/2}\sum_{n=1}^{\infty}(-1)^n\left(\left(\frac{r}{R}\right)^{2n}-1\right) \times\left(n!n\left(\frac{w}{R}\right)^{2n}\right)^{-1} r\,dr\,dz \tag{9}$$

and

$$D_m = \frac{4}{R^2L}\int_0^R\int_0^{L/2} C_m J_0\left(\xi_m\frac{r}{R}\right)r\,dr\,dz. \tag{10}$$

L is the length of the cylindrical sample space. Equation (8) leads to

$$\Delta\bar{T}(t) = \left(\frac{\alpha WB}{4\pi\lambda}\right)\left[1+\sum_{m=1}^{\infty} K_m\exp\left(-\frac{\xi_m^2 at}{R^2}\right)\right] \tag{11}$$

with

$$K_m = \frac{D_m}{B}. \tag{12}$$

The parameter B and the coefficients D_m ($m = 1, 2, \ldots, \infty$) are obtained from equations (9), (10), and (3). Numerical integration yields $B = 0.921208$ and the values of D_m and K_m given in Table 1. From equation (11) one obtains the average temperature rise for infinite time:

$$\Delta\bar{T}_\infty = \Delta\bar{T}(t\to\infty) = \frac{\alpha WB}{4\pi\lambda}. \tag{13}$$

With this, equation (11) can be written

$$\Delta\bar{T}(t) = \Delta\bar{T}_\infty\left[1+\sum_{m=1}^{\infty} K_m\exp\left(-\frac{\xi_m^2 at}{R^2}\right)\right]. \tag{14}$$

The temperature rise $\Delta\bar{T}(t)$ is related to the pressure rise $\Delta p(t) = p(t)-p_0$. From a Taylor series we obtain

Table 1. Values of coefficients D_m and K_m according to equations (10) and (12)

m	D_m	K_m
1	−0.988732	−1.073299
2	+0.076692	+0.083252
3	−0.010403	−0.011292
4	+0.001357	+0.001473
5	−0.000144	−0.000156
6	+0.000012	+0.000013

$$\bar{T}(t) = T_0 + \left(\frac{\partial T}{\partial p}\right)_{p_0, T_0} \Delta p(t) + \frac{1}{2}\left(\frac{\partial^2 T}{\partial p^2}\right)_{p_0, T_0} \Delta p(t)^2 + \cdots \quad (15)$$

where p_0, T_0 stand for the initial state. The pressure rise $\Delta p(t)$ is only a few Pa and thus very small compared to the system pressure p_0. In our experiments we use fluids with ideal or weak real gas behavior. The value of $(\partial^2 T/\partial p^2)_{p_0, T_0}$ is small for weak real gases and $(\partial^2 T/\partial p^2)_{p_0, T_0} = 0$ for ideal gases. Therefore it follows that

$$\left(\frac{\partial T}{\partial p}\right)_{p_0, T_0} \Delta p(t) \gg \frac{1}{2}\left(\frac{\partial^2 T}{\partial p^2}\right)_{p_0, T_0} \Delta p(t)^2$$

and equation (15) can be written as

$$\Delta \bar{T}(t) = \bar{T}(t) - T_0 = \left(\frac{\partial T}{\partial p}\right)_{p_0, T_0} \Delta p(t) \quad (16)$$

and in particular for infinite time

$$\Delta \bar{T}(t \to \infty) = \Delta \bar{T}_\infty = \left(\frac{\partial T}{\partial p}\right)_{p_0, T_0} \Delta p_\infty. \quad (17)$$

From equations (16) and (17) it follows that

$$\frac{\Delta \bar{T}(t)}{\Delta \bar{T}_\infty} = \frac{\Delta p(t)}{\Delta p_\infty} \quad (18)$$

and from equation (14) we obtain the time-dependent pressure rise

$$\Delta p(t) = \Delta p_\infty \left[1 + \sum_{m=1}^{i} K_m \exp\left(-\frac{\xi_m^2 at}{R^2}\right)\right]. \quad (19)$$

From the measured pressure rise, as for the example in Fig. 4, the thermal diffusivity a can be evaluated by equation (19). The signal amplitude Δp_∞ can be determined directly from the measured photoacoustic signal. However, random acoustic noise superimposed to the signal would provoke an error of Δp_∞ and thus lead to inaccuracies of the thermal diffusivity from equation (19). Instead, we fitted Δp_∞ to the measured pressure rise and thus achieved better accuracy of the thermal diffusivity.

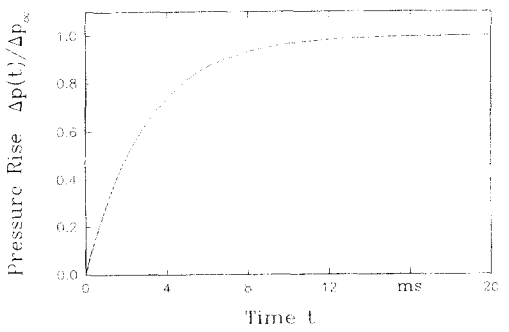

FIG. 4. Normalized pressure rise vs time.

4. EXPERIMENTAL APPARATUS

The experimental apparatus is shown schematically in Fig. 5. Coherent light of a constant wavelength of 3.4 μm is produced by a helium–neon laser. The laser beam is periodically modulated by a mechanical chopper, which itself is placed in a closed box in order to prevent disturbances by sound transmission of the chopper blade and vibrations of the chopper motor from the microphone. In order to obtain a maximum radiation intensity within the sample chamber, the laser beam is focussed by two CaF_2 lenses with focal lengths $f_1 = 300$ mm and $f_2 = 100$ mm. The radiation energy is partially absorbed by the sample gas in the photoacoustic cell. The cell itself has to be adjusted to attain coincidence of the beam axis and the axis of the sample tube. The adjustment had to be verified carefully by measuring the intensity profile of the outcoming beam with a beam scanner.

The photoacoustic cell (Fig. 6) consists of the sample chamber inside a copper cylinder and the microphone compartment. The sample chamber designed for experiments up to 423 K had to be separated from the microphone in order to protect it from high temperatures and direct illumination. A stainless steel tube with an inner diameter of 1.535 mm and a length of 100 mm served as sample chamber. This tube was shrunk into the copper cylinder to attain good thermal contact. CaF_2 windows permitting nearly 100% transmission of the infrared laser light enclose the sample chamber. The copper cylinder contains heating filaments at its jacket and at the front sides so that a constant wall temperature can be maintained. In addition, the windows are placed in a cavity of the cylinder to prevent heat losses by radiation and convection. The temperature of the sample compartment is regulated with a PID-controller and a platinum resistance thermometer. The sample chamber is connected to the microphone chamber by an acoustic coupling tube. Such a configuration forms a Helmholtz resonator [12, 13] and can lead to undesired oscillations superimposed to the photoacoustic signal. The frequency of these oscillations depends on the length and the inner diameter of the coupling tube, the size of the two chambers, and the speed of sound of the sample gas [14]. We designed the coupling tube with an inner diameter of 4.6 mm and a length of 100 mm. This leads to frequencies more than 15 times higher than the chopping frequency and to low amplitudes of the disturbing oscillations. They can be partially suppressed by a low noise filter, but the remaining disturbance signal still slightly affects the accuracy of the measurements. A larger diameter of the coupling tube would lead to higher frequencies but lower amplitudes of the photoacoustic signal and thus deteriorate the signal-to-noise ratio. The microphone chamber is placed slightly below the heated sample chamber so that convection between the two chambers is prevented. Capillary tubes connect the microphone chamber with valves for evacuating and filling the cell with sample gas.

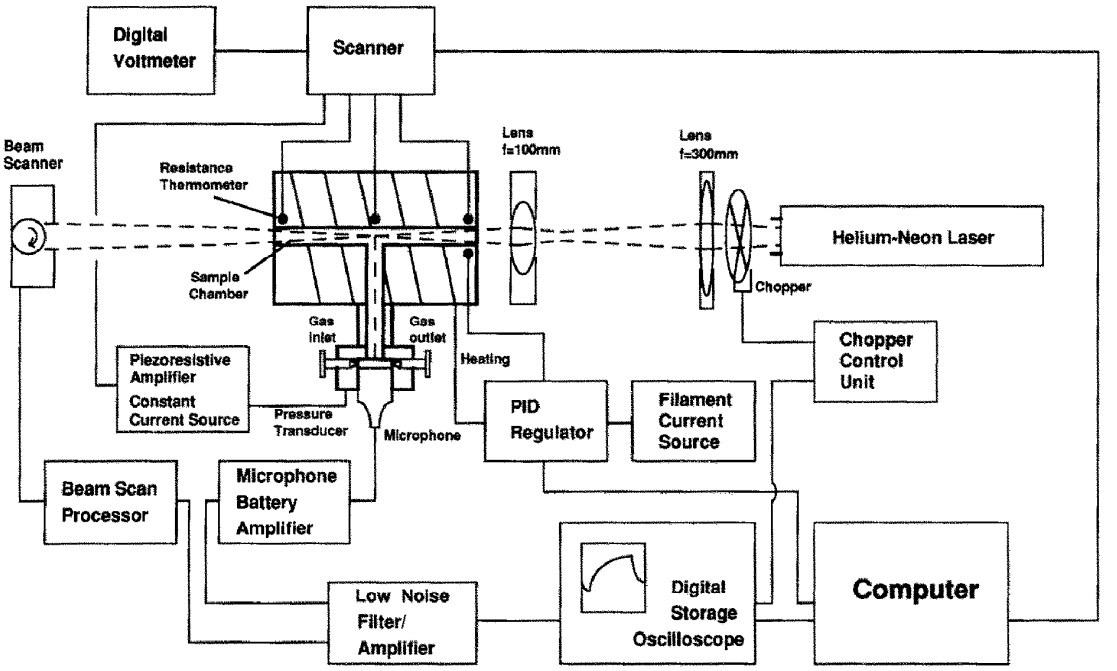

FIG. 5. Experimental apparatus.

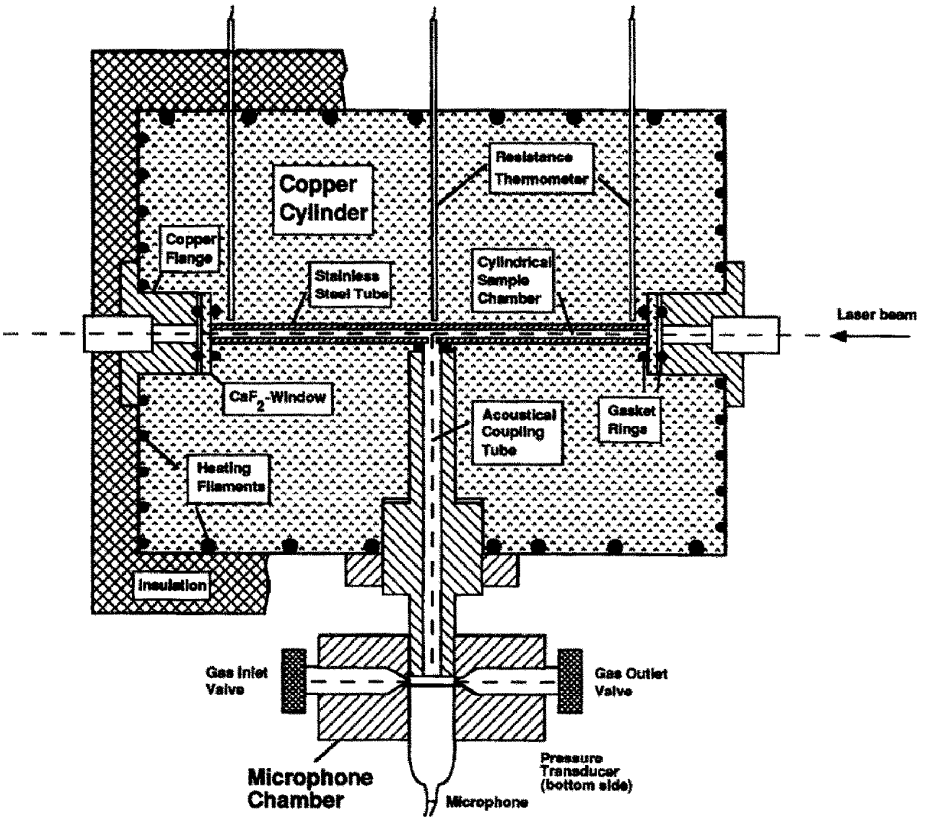

FIG. 6. Photoacoustic cell.

The system pressure is measured with a piezoresistive pressure transducer (Kistler 4043 A1) mounted into the microphone compartment. Calibration of the pressure transducer, the constant current source supplying the measuring bridge, and the differential voltage amplifier leads to an overall error of the measured system pressure below 0.4%. The temperature T_0 of the cylindrical sample chamber is determined in the center of the cell and at the ends of the sample space by calibrated platinum resistance thermometers with an error less than 0.1 K.

A condenser microphone (Bruel & Kjaer 4144) closely connected to a preamplifier detects the photoacoustic signal, which, after additional amplification and filtering, is digitized and monitored by a 12-bit storage oscilloscope.

5. EXPERIMENTAL RESULTS

For examination of the precision of thermal diffusivity measurements we used argon as the reference fluid. About 180 measurements were carried out at atmospheric pressure in the temperature range between 295 and 423 K. At each temperature between five and ten data points were taken. Evaluation of the measured data included a careful examination of the acoustic noise superimposed to the signal. As the thermal conductivity of argon is well known, reference data can easily be calculated from equation (7). The isochoric heat capacity in this equation was obtained from

$$c_v = \frac{1}{\kappa - 1}\frac{\mathbb{R}}{M} \tag{20}$$

with the universal gas constant $\mathbb{R} = 8.3143$ J mol^{-1} K^{-1}, the molar mass of argon $M = 39.948$ kg kmol^{-1}, and the isentropic exponent $\kappa = 1.6667$ for noble gases. The density can be calculated from the equation of state for ideal gases. Thermal conductivities were determined from a correlation of Bich *et al.* [15] based on an improved kinetic theory for moderately dense gases. A relative uncertainty of 0.5% is given for their correlated data at 300 K. Comparison with other correlations [16, 17] demonstrates good agreement, in particular for the thermal conductivity of argon.

Table 2 contains experimental results obtained for 27 isotherms; the mean value of the measurements for each isotherm is given, together with the standard deviation and the maximum deviation from the mean value. The standard deviation is of the order of 0.5–1% for all isotherms, whereas the maximum deviation from the mean values does not exceed 1.5%. A slight deterioration of the reproducibility at temperatures above 373 K can be explained by a smaller signal-to-noise ratio due to the decrease of the signal amplitude and the slight increase in acoustic noise at higher

Table 2. Mean values of measured thermal diffusivities for 27 isotherms with standard deviation and maximum deviation from the mean values

Temperature T (K)	Pressure p (MPa)	Thermal diff. experimental $\bar{a}_{exp}$ (10^{-6} m^2 s^{-1})	Standard deviation (%)	Maximum deviation (%)
294.9	0.1035	33.27	0.15	−0.26
298.6	0.1035	34.19	0.20	0.28
303.3	0.1035	34.90	0.51	−0.70
308.7	0.1036	36.04	0.36	0.49
313.3	0.1037	36.89	0.47	−0.72
318.1	0.1036	38.19	0.36	0.56
323.0	0.1036	39.32	0.61	−0.93
328.1	0.1035	40.27	0.84	−1.07
333.3	0.1036	41.66	0.45	0.69
338.3	0.1036	42.83	0.42	0.63
343.2	0.1036	44.10	0.77	1.02
348.1	0.1036	45.20	0.48	0.58
353.2	0.1035	46.42	0.71	−1.24
358.2	0.1035	47.88	0.58	−0.77
363.1	0.1035	48.54	0.47	−0.51
368.1	0.1038	49.63	0.65	1.10
373.3	0.1042	50.83	1.03	−1.31
378.3	0.1046	52.01	1.01	−1.38
383.2	0.1049	53.01	0.83	−1.42
388.1	0.1053	54.56	0.26	−0.27
392.9	0.1058	55.50	0.50	−0.61
397.9	0.1062	56.64	0.50	−0.52
402.9	0.1065	57.65	0.53	−0.90
408.1	0.1069	58.52	0.75	−1.05
413.3	0.1071	59.56	0.71	−0.98
418.2	0.1072	61.04	0.73	−1.18
423.2	0.1074	61.86	1.08	1.40

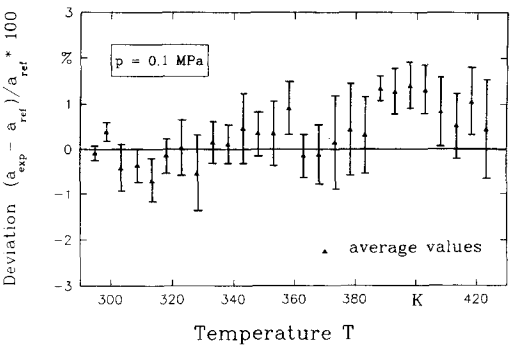

FIG. 7. Average values of measured thermal diffusivities with standard deviation for 27 isotherms compared to reference data.

temperatures. From the reproducibility of the thermal diffusivity measurements we estimate a precision of the order of 1%.

The deviation of the experimental data compared to reference data is shown in Fig. 7. The average absolute deviation of thermal diffusivity measurements compared to the reference data is 0.5% for temperatures below 373 K and 1.0% for temperatures above 373 K.

6. CONCLUSIONS

A photoacoustic cell for accurate determination of thermal diffusivities of gases in the temperature range between 290 and 423 K at atmospheric pressure is described. An analysis of the effect leads to an equation for the time-dependent photoacoustic signal whereby the thermal diffusivity can be evaluated.

In order to verify the reproducibility of thermal diffusivity measurements attainable with the experimental set-up, measurements were performed with argon as the reference fluid. According to the experimental results a precision of approximately 1% was estimated. The average absolute deviation from the best available reference data is 0.5% below 373 K and 1.0% between 373 and 423 K.

The present results prove the photoacoustic technique to be a promising method for determining thermal diffusivities of gases, especially in the range of low densities where other experimental techniques, e.g. the transient hot-wire technique and the method of dynamic light scattering, are not applicable or do not provide satisfactory results.

Acknowledgement—We gratefully acknowledge the financial support by the Deutsche Forschungsgemeinschaft.

REFERENCES

1. P. G. Knibbe and R. D. Raal, Simultaneous measurement of the thermal conductivity and thermal diffusivity of liquids, *Int. J. Thermophys.* **8,** 181–191 (1987).
2. Y. Nagasaka and A. Nagashima, Simultaneous measurement of the thermal conductivity and the thermal diffusivity of liquids by the transient hot-wire method, *Rev. Sci. Instrum.* **52,** 229–232 (1981).
3. B. Kruppa, P. Jany and J. Straub, Experimental apparatus for measuring the thermal diffusivity of pure fluids at high temperatures, *Int. J. Thermophys.* **9,** 911–921 (1988).
4. P. Jany and J. Straub, Thermal diffusivity of fluids in a broad region around the critical point, *Int. J. Thermophys.* **8,** 165–180 (1987).
5. A. Leipertz, G. Wu and M. Fiebig, Spectroscopic determination of the thermal diffusivity of organic mixtures and refrigerants, *Proc. Int. Centre for Heat and Mass Transfer*, Belgrade, Vol. 24, pp. 393–403 (1987).
6. A. Leipertz, Transport properties of transparent liquids by photon-correlation spectroscopy, *Int. J. Thermophys.* **9,** 897–909 (1988).
7. C. A. Nieto de Castro, B. Taxis, H. M. Roder and W. A. Wakeham, Thermal diffusivity measurement by the transient hot-wire technique: a reappraisal, *Int. J. Thermophys.* **9,** 293–316 (1988).
8. B. Kruppa and J. Straub, Measurement of thermal diffusivity of the refrigerants R22 and R134a by means of dynamic light scattering, Paper presented at the *11th Symp. on Thermophysical Properties*, Boulder, CO, U.S.A. (23–27 June 1991).
9. K. Stephan, V. Rothacker and W. Hurdelbrink, Thermal diffusivities determined by photoacoustic spectroscopy, *Chem. Engng Process.* **26,** 257–261 (1989).
10. H. Kogelnik and T. Li, Laser beams and resonators, *Appl. Opt.* **5,** 1550–1567 (1966).
11. E. L. Kerr and J. G. Atwood, The laser illuminated spectrophone: a method for measurement of weak absorptivity in gases at laser wavelengths, *Appl. Opt.* **7,** 915–921 (1968).
12. O. Nordhaus and J. Pelzl, Frequency dependence of resonant photoacoustic cells: the extended Helmholtz resonator, *Appl. Phys.* **25,** 221–229 (1981).
13. J. Pelzl, K. Klein and O. Nordhaus, Extended Helmholtz resonator in low-temperature photoacoustic spectroscopy, *Appl. Opt.* **21,** 94–99 (1982).
14. N. C. Fernelius, Helmholtz resonance effect in photoacoustic cells, *Appl. Opt.* **18,** 1784–1787 (1979).
15. E. Bich, J. Millat and E. Vogel, The viscosity and thermal conductivity of pure monatomic gases from their normal boiling point up to 5000 K in the limit of zero density and at 0.101325 MPa, *J. Phys. Chem. Ref. Data* **19,** 1289–1305 (1990).
16. J. Kestin, K. Knierim, A. Mason, B. Najafi, S.T. Ro and M. Waldmann, Equilibrium and transport properties of the noble gases and their mixtures at low density, *J. Phys. Chem. Ref. Data* **13,** 229–303 (1984).
17. B. A. Younglove and H. J. M. Hanley, The viscosity and thermal conductivity coefficients of gaseous and liquid argon, *J. Phys. Chem. Ref. Data* **15,** 1323–1337 (1986).

LA TECHNIQUE PHOTOACOUSTIQUE COMME MOYEN DE DETERMINATION DES DIFFUSIVITES THERMIQUES DES GAZ

Résumé—La diffusivité thermique de l'argon gazeux est déterminée par une méthode basée sur l'effet photoacoustique. Les fondements théoriques de la technique photoacoustique pour la mesure de la diffusivité thermique sont présentés et on décrit une cellule photoacoustique conçue pour des mesures précises dans le domaine de température depuis 290 jusqu'à 423 K, à la pression atmosphérique. La déviation absolue moyenne des données expérimentales par rapport aux données recommandées ne dépasse pas 1%.

EINE PHOTOAKUSTISCHE MEßMETHODE ZUR BESTIMMUNG DER TEMPERATURLEITFÄHIGKEIT VON GASEN

Zusammenfassung—Die Temperaturleitfähigkeit von Gasen kann man mit einem Verfahren messen, das auf dem photoakustischen Effekt beruht. Die theoretischen Grundlagen des photoakustischen Verfahrens zur Bestimmung von Temperaturleitfähigkeiten werden vorgestellt, und es wird eine photoakustische Meßzelle für Messungen im Temperaturbereich zwischen 290 und 423 K beschrieben. Die mittlere absolute Abweichung der gemessenen Temperaturleitfähigkeiten von Argon von den besten Referenzdaten ist kleiner als 1%.

ФОТОАКУСТИЧЕСКИЙ МЕТОД ОПРЕДЕЛЕНИЯ ТЕМПЕРАТУРОПРОВОДНОСТИ ГАЗОВ

Аннотация—С использованием метода, базирующегося на фотоакустическом эффекте, определяется температуропроводность газообразного аргона. Приводятся теоретические основы этого метода и описывается фотоакустический элемент, предназначенный для точных измерений в интервале температур от 290 до 423 К при атмосферном давлении. Среднее отклонение экспериментальных данных от известных не превышает 1%.